Unitary *p*-wave interactions between fermions in an optical lattice

https://doi.org/10.1038/s41586-022-05405-6

Received: 15 May 2022

Accepted: 3 October 2022

Vijin Venu[1,5], Peihang Xu[1,5], Mikhail Mamaev[2,3], Frank Corapi[1], Thomas Bilitewski[2,3,4], Jose P. D'Incao[2], Cora J. Fujiwara[1]✉, Ana Maria Rey[2,3]✉ & Joseph H. Thywissen[1]✉

Exchange-antisymmetric pair wavefunctions in fermionic systems can give rise to unconventional superconductors and superfluids[1–3]. The realization of these states in controllable quantum systems, such as ultracold gases, could enable new types of quantum simulations[4–8], topological quantum gates[9–11] and exotic few-body states[12–15]. However, *p*-wave and other antisymmetric interactions are weak in naturally occurring systems[16,17], and their enhancement via Feshbach resonances in ultracold systems has been limited by three-body loss[18–24]. Here we create isolated pairs of spin-polarized fermionic atoms in a multiorbital three-dimensional optical lattice. We spectroscopically measure elastic *p*-wave interaction energies of strongly interacting pairs of atoms near a magnetic Feshbach resonance. The interaction strengths are widely tunable by the magnetic field and confinement strength, and yet collapse onto a universal curve when rescaled by the harmonic energy and length scales of a single lattice site. The absence of three-body processes enables the observation of elastic unitary *p*-wave interactions, as well as coherent oscillations between free-atom and interacting-pair states. All observations are compared both to an exact solution using a *p*-wave pseudopotential and to numerical solutions using an ab initio interaction potential. The understanding and control of on-site *p*-wave interactions provides a necessary component for the assembly of multiorbital lattice models[25,26] and a starting point for investigations of how to protect such systems from three-body recombination in the presence of tunnelling, for instance using Pauli blocking and lattice engineering[27,28].

The emergent behaviour of a quantum many-body system is fundamentally tied to the quantum statistics of its constituents. For pairs of identical fermions, the wavefunction must be exchange antisymmetric, which is found only in odd-L pairwise collision channels, where L is orbital angular momentum. Despite a well-understood connection between odd-L interactions and topological properties[2,4–6,8,9,11,29], liquid ^{3}He remains the only laboratory example of well-established *p*-wave ($L = 1$) interactions. The discovery of tunable *p*-wave interactions in ultracold atoms[18,20] was promising, but experimental efforts have so far been severely limited by enhanced three-body recombination, a process whereby three atoms collide to form a diatomic molecule, releasing enough kinetic energy to make all products escape confinement[18–24]. The essential challenge for $L > 0$ systems is that wavefunction amplitude at short internuclear separation, where recombination processes are strong, is enhanced by centrifugal kinetics. Progress has been made in understanding few-body correlations[7,12–15] and developing proposals towards overcoming this obstacle via wavefunction engineering[27], including low-dimensional confinement[30,31]. Still, *p*-wave interaction energies between free atoms are yet to be measured directly or compared to predictions of any theory. Even at the level of two particles, the description of *p*-wave interactions by a Feshbach-tuned, energy-dependent scattering volume $\upsilon(\mathcal{E})$[32,33] has yet to be tested experimentally.

In this article, we report the first direct measurement and coherent control of the elastic *p*-wave interaction between two identical fermions in a multiorbital lattice. Central to this advance is the use of strong three-dimensional confinement to modify the wavefunction and to suppress three-body processes. Interactions are tuned using the magnetic Feshbach coupling[6] between free-atom pairs and a molecular dimer channel. Our spectral resolution and orbital control allow us to transfer pairs of weakly interacting ^{40}K atoms into strongly interacting two-atom complexes whose energies and wavefunctions separate them into repulsive and attractive branches. Within the two lowest branches we are able to reach the unitary limit, where $\upsilon(\mathcal{E})$ diverges. We demonstrate the coherence of the conversion process between non-interacting and strongly interacting atomic pairs by measuring Rabi oscillations between them, and find an oscillation frequency consistent with theory. Finally, we demonstrate that losses in the upper branch are limited by the intrinsic lifetime of the ^{40}K molecular dimer, and we measure lifetimes that are 50 times larger than observed previously for weakly confined *p*-wave dimers of ^{40}K[34].

---

[1]Department of Physics and CQIQC, University of Toronto, Toronto, Ontario, Canada. [2]JILA, NIST and Department of Physics, University of Colorado, Boulder, CO, USA. [3]Center for Theory of Quantum Matter, University of Colorado, Boulder, CO, USA. [4]Department of Physics, Oklahoma State University, Stillwater, OK, USA. [5]These authors contributed equally: Vijin Venu, Peihang Xu. ✉e-mail: cora.fujiwara@utoronto.ca; arey@jila1.colorado.edu; joseph.thywissen@utoronto.ca

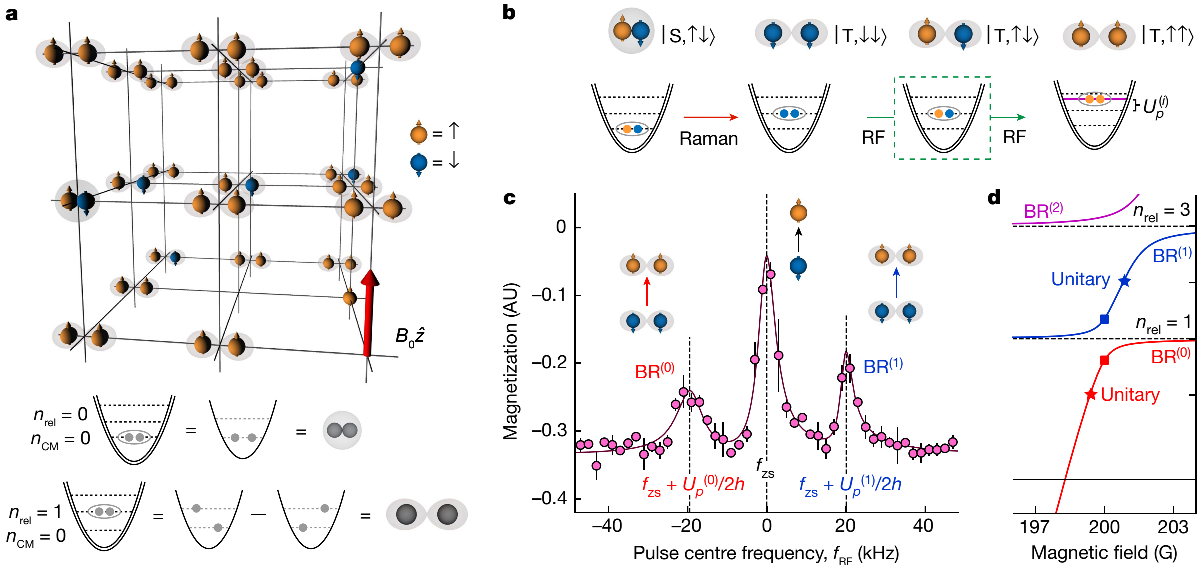

Fig. 1 | Spectroscopy of *p*-wave interactions between spin-polarized fermions. a, Atoms with ↑ or ↓ spin are loaded into a harmonic-trap array formed by a deep three-dimensional optical lattice. The double-struck parabola represents the two-atom n_{rel} motional degree of freedom. Pairs of atoms are shown in the non-interacting ground ($n_{rel} = n_{CM} = 0$) or first excited ($n_{rel} = 1, n_{CM} = 0$) motional mode. An applied magnetic field ($B_0\hat{\mathbf{z}}$) creates the Feshbach coupling between ↑ atoms. **b**, Measurement protocol. An optical Raman π-pulse converts singlet |S, ↑↓⟩ pairs in the ground motional state into |T, ↓↓⟩ with a motional excitation $n_{rel} = 1$. An RF sweep, centred at f_{RF}, then transfers some pairs to the interacting |T, ↑↑⟩ state through a two-RF-photon process. The off-resonant intermediate state |T, ↑↓⟩ is shown in the dashed box. **c**, The measured magnetization (here, at magnetic field 200.00(1) G and trap angular frequency $\omega = 2\pi \times 129(2)$ kHz) exhibits three distinct spectroscopic features for varying RF centre frequency. The leftmost and rightmost peaks correspond to transitions to interacting states in the $BR^{(0)}$ and $BR^{(1)}$ branches, with interaction energies $U_p^{(0)}$ and $U_p^{(1)}$, as labelled. The solid line is a best-fit spectral function. Error bars represent the standard deviation of repeated measurements. **d**, The spectrum of interacting |T, ↑↑⟩ pairs after subtracting the energy associated with the free-atom magnetic moments. The spectrum reflects mixing of the odd-n_{rel} harmonic states with a magnetic dimer state. Coloured squares indicate the spectral peak locations from **c**, and stars indicate points with unitary *p*-wave interactions. AU, arbitrary units.

Our optical lattice system realizes an array of isotropic harmonic traps, each occupied by a pair of atoms with spin and orbital degrees of freedom (Fig. 1a). The spin state of a pair is $|\mathcal{S}, M_{\mathcal{S}}\rangle$, where $\mathcal{S} = \{\mathrm{S}, \mathrm{T}\}$ indicates either singlet or triplet spin symmetry, $M_{\mathcal{S}} = \{\uparrow\uparrow, \downarrow\downarrow, \uparrow\downarrow\}$ are projections on the magnetic field axis, and ↑ and ↓ are the lowest hyperfine states of ^{40}K. Tunable enhancement of *p*-wave interactions is provided by a Feshbach resonance for spin-symmetric pairs |T, ↑↑⟩ (Methods). The motional state of a pair is described by the relative and centre-of-mass mode numbers $n_{rel} = \{0, 1, \ldots\}$ and $n_{CM} = \{0, 1, \ldots\}$, respectively. The centre of mass decouples from the collisional interactions and remains in its motional ground state, $n_{CM} = 0$. The relative mode number is $n_{rel} = 2\mathcal{N} + L$, where $\mathcal{N}$ is the conventional radial excitation number for a spherical harmonic oscillator. As the overall pair state must have odd exchange symmetry and the interacting spin state |T, ↑↑⟩ is even, the motional state must have odd L, which implies $n_{rel} = 1, 3, \ldots$ for $L = 1$ (*p*-wave). This is in contrast to *s*-wave-interacting spin singlet states, which can interact when prepared in the least energetic motional mode ($n_{rel} = n_{CM} = 0$)[35,36].

The magnetic field-dependent eigenstates of a |T, ↑↑⟩ pair can be understood as the coupling of the odd-n_{rel} motional modes to a molecular state. We sketch the spectrum of the interacting pair in Fig. 1d. For fields far below the Feshbach resonance, the spectrum is given by a ladder with harmonic spacing $2\hbar\omega$ (corresponding to $n_{rel} = 1, 3, \ldots$), where ω is the trap angular frequency, and a molecular dimer state whose energy depends linearly on magnetic field. As each motional mode becomes near resonant with this dimer, the Feshbach coupling imparts a *p*-wave interaction energy shift and mixes the harmonic states. We label the resulting eigenstates of the interacting pair as branches $\{BR^{(0)}, BR^{(1)}, BR^{(2)} \ldots\}$ in order of increasing energy $\mathcal{E}^{(i)}$. In this work, we probe the lowest energy branches, $BR^{(0)}$ and $BR^{(1)}$. As they are both adiabatically connected to the $n_{rel} = 1$ mode, we use it as a common reference to define the on-site interaction energies $U_p^{(i)}$, that is, $\mathcal{E}^{(0)} = U_p^{(0)} + \frac{5}{2}\hbar\omega$ and $\mathcal{E}^{(1)} = U_p^{(1)} + \frac{5}{2}\hbar\omega$.

We assemble the desired pair states by orbital excitation of a low-entropy spin mixture. First, |S, ↑↓⟩ pairs in the lowest motional mode ($n_{rel} = n_{CM} = 0$) are created by loading a spin-balanced degenerate Fermi gas into a three-dimensional optical lattice of moderate depth (Methods). The lattice depth is then rapidly increased, which isolates atom pairs and prevents undesired three-body processes. An orbital excitation accompanied by a spin flip is created by a π-pulse from optical Raman beams[37], whose detuning from the electronic excited state is chosen to minimize photoassociative loss of pairs (Methods). The pulse transforms |S, ↑↓⟩ pairs into the spin-symmetric state |T, ↓↓⟩ with a relative orbital excitation $n_{rel} = 1$ (Fig. 1b).

Having engineered the required spin symmetry and orbital excitation, we can create and measure strong *p*-wave interactions via radio-frequency (RF) manipulation. The double-spin-flip resonance condition between |T, ↑↑⟩ and |T, ↓↓⟩ is $2f_{RF} = 2f_{ZS} + U_p^{(i)}/h$, where f_{RF} is the centre frequency of the RF pulse, f_{ZS} is the Zeeman splitting of ↑ and ↓ spins, and h is Planck's constant. At resonance, the pulse transfers |T, ↓↓⟩ pairs to |T, ↑↑⟩ through a second-order process via the virtual state |T, ↑↓⟩ (Fig. 1b). Spin flips induced by the RF pulse are detected as changes in the ensemble magnetization obtained via time-of-flight imaging (Methods). Figure 1c shows repeated measurements with variable f_{RF} and features three distinct spin-resonance peaks. The central feature corresponds to flipping an isolated (and thus non-interacting) spin and is used to calibrate the magnetic field strength. The two side features indicate successful transfers of |T, ↓↓⟩ pairs to interacting |T, ↑↑⟩ pair states in $BR^{(0)}$ and $BR^{(1)}$ with interaction energies $U_p^{(0)} < 0$ and $U_p^{(1)} > 0$, respectively. The observed spectra, such as Fig. 1c, constitute the first direct measurements of the elastic *p*-wave interaction energy in isolated pairs,

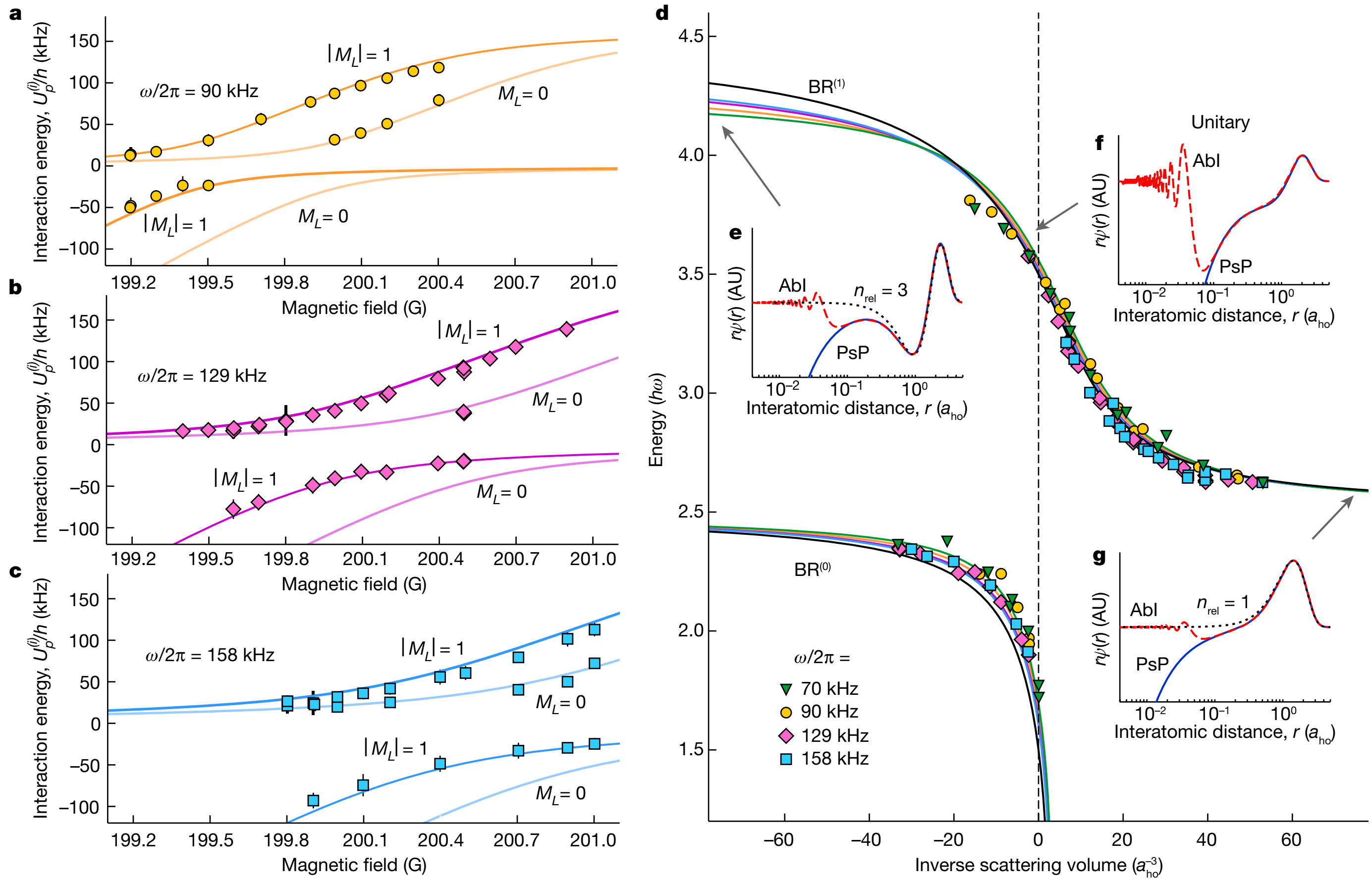

Fig. 2 | Characterization of unitary and elastic *p*-wave interactions. **a**–**c**, The measured interaction energies (points) are shown versus magnetic field at three different trap frequencies *ω*, as labelled. Vertical error bars are full-width at half-maximum (FWHM) values from the best-fit spectral function. Solid lines are the PsP predictions for orbital angular momentum projections $M_L = -1, 0, 1$, including anharmonic corrections (Methods). **d**, When scaled by the harmonic oscillator angular frequency, the measured energies collapse onto a single universal curve as a function of inverse scattering volume, in units of the oscillator length $a_{\rm ho}$. The black solid line is the harmonic PsP energy, and the coloured solid lines include anharmonic corrections, which are weakly sensitive to lattice depth. **e**–**g**, Representative spatial wavefunctions of the interacting pairs calculated for weakly attractive ($v(\mathcal{E})^{-1} = -200\,a_{\rm ho}^{-3}$) (**e**), near-unitary ($v(\mathcal{E})^{-1} = -5\,a_{\rm ho}^{-3}$) (**f**) and weakly repulsive ($v(\mathcal{E})^{-1} = 270\,a_{\rm ho}^{-3}$) (**g**) conditions. The solid blue lines are obtained from the PsP, and the red dashed lines from an AbI calculation (see Methods). The short-range divergence of the PsP wavefunction requires a cut-off to be normalizable. As **e** and **g** are in the non-interacting limit with $n_{\rm rel} = 3$ and $n_{\rm rel} = 1$ motional quanta, respectively, the corresponding oscillator states are shown as black dotted lines. Panel **f** corresponds to the unitary limit of divergent $v(\mathcal{E})$.

complementing prior measurements of molecular binding energies in bulk[34,38].

We probe the eigenspectrum of interacting *p*-wave atoms through RF spectroscopic scans at various trap frequencies and magnetic fields. The measured energies test the validity of an analytical treatment that uses the *p*-wave pseudopotential[32,33] (PsP) to calculate the interaction energy as a function of the energy-dependent scattering volume, $v(\mathcal{E})$ (Methods). At unitarity, $v(\mathcal{E})$ diverges, but the interaction energy remains finite with $U_p^{(0)} = -\hbar\omega$ and $U_p^{(1)} = +\hbar\omega$. This resonant behaviour, in which the energy is independent of the microscopic details of the atomic interaction, is universal to harmonically trapped systems[33,39]. As shown in Fig. 1d, different branches of the energy spectrum attain unitarity at distinct magnetic fields that differ from the free-space resonance due to the energy dependence of the scattering volume. In Fig. 2a–c we compare the measured interaction energy to the PsP prediction, including a leading-order anharmonic correction (Methods). In both branches, we observe agreement across a wide range of interaction strengths, including in the unitary limit with the measured interaction energies attaining ± ħ*ω* for various trap frequencies. Figure 2d collects all data as $\mathcal{E}/\hbar\omega$ versus $a_{\rm ho}^3/v(\mathcal{E})$, where $a_{\rm ho} = \sqrt{\hbar/\mu\omega}$ is the harmonic oscillator length, $\mu = m/2$ is the reduced mass and *m* is the atomic mass. The data collapse demonstrates the exclusive dependence of *p*-wave interaction energies on a single parameter, which implies the universal applicability of this result to any *p*-wave interacting system in the tight-binding limit.

Further insight is provided by comparing the wavefunctions of the PsP theory to those obtained numerically from an ab initio (AbI) interaction potential specific to ^{40}K (Fig. 2e–g). At short length scales $r \lesssim 0.1\,a_{\rm ho}$, which correspond to the characteristic size of the Feshbach molecular state, the PsP diverges while the AbI does not. However, as described in the Supplementary Information, after regularization with a short-range cut-off (at the van der Waals length), the PsP wavefunction is normalizable and accurately predicts the long-range wavefunction. Far from resonance, both the PsP and AbI wavefunctions match the non-interacting oscillator states ($n_{\rm rel} = 1$ in Fig. 2g and $n_{\rm rel} = 3$ in Fig. 2e).

Next, we demonstrate coherent manipulation of *p*-wave interacting pairs, which also probes the interacting wavefunctions. As shown in Fig. 3a, application of RF radiation under the two-photon resonance condition for the BR$^{(1)}$ branch results in an oscillating ensemble magnetization with a two-tone frequency character. The faster oscillation evident at short times corresponds to (off-resonant) ↑-to-↓ Rabi oscillations of single spins (Fig. 3b); the slower oscillation persisting for longer time corresponds to resonant Rabi oscillations of pairs between $|T, \downarrow\downarrow\rangle$ and $|T, \uparrow\uparrow\rangle$ (Fig. 3c). The oscillation frequency of the pairs is

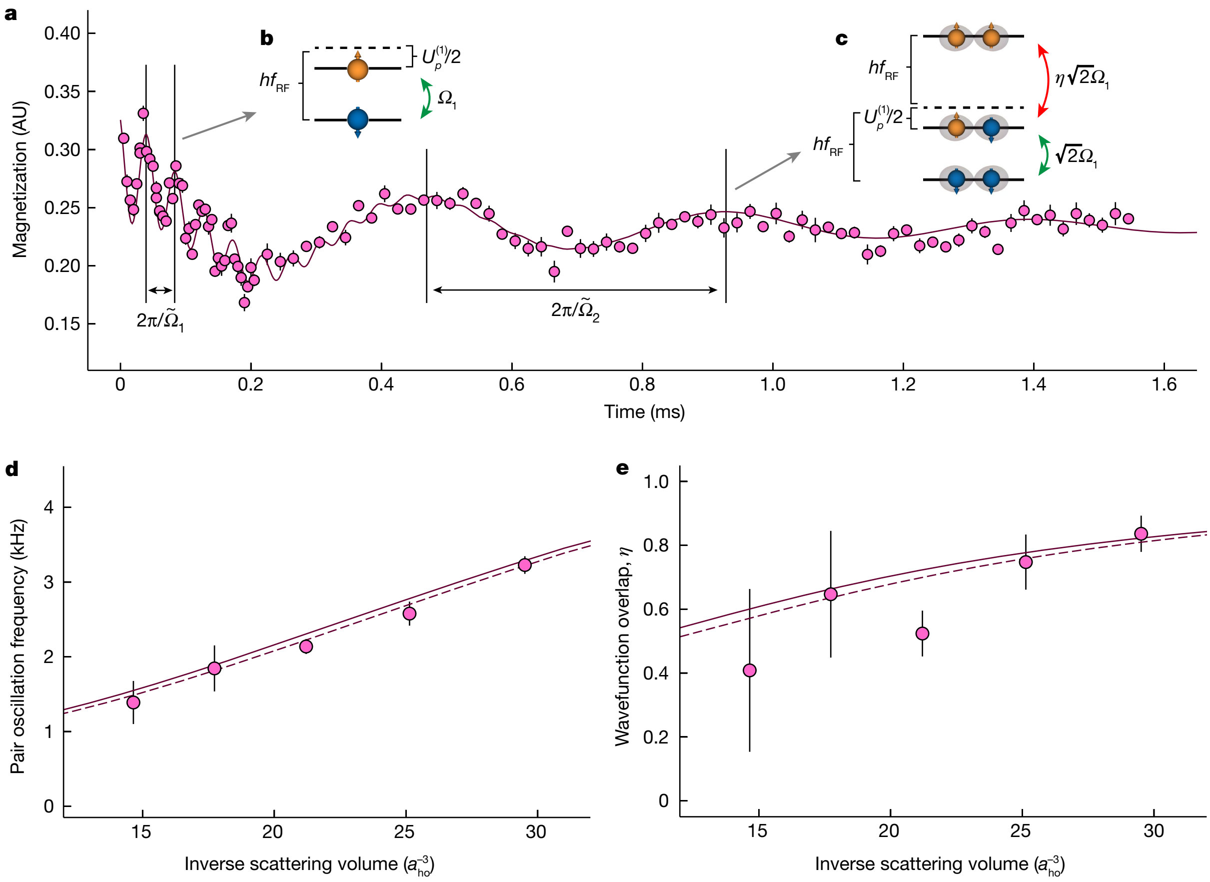

Fig. 3 | Coherent manipulation of *p*-wave interacting pairs. a, Temporal oscillations in the magnetization are observed when applying an RF drive resonant with the two-photon |T, ↓↓⟩ to |T, ↑↑⟩ transition. Here, the trap angular frequency is $\omega = 2\pi \times 129(2)$ kHz, and the magnetic field is 200.00(1) G. A boxcar average with a 50 μs window is applied to the data for times less than 200 μs for visual clarity. Error bars are the standard deviation of repeated data points. A two-frequency fit finds $\tilde{\Omega}_1 = 2\pi \times 22.7(4)$ kHz and $\tilde{\Omega}_2 = 2\pi \times 2.15(4)$ kHz, which we identify as one- and two-atom processes, respectively. **b**, Rabi oscillations caused by off-resonant coupling of single spins should occur with generalized Rabi frequency $\tilde{\Omega}_1 = \sqrt{\Omega_1^2 + (U_p^{(1)}/(2\hbar))^2}$. An independent calibration gives the single-particle Rabi frequency $\Omega_1 = 2\pi \times 8.83(2)$ kHz. **c**, Rabi oscillations caused by on-resonant two-photon coupling of |T, ↓↓⟩ to |T, ↑↑⟩ occur with frequency $\tilde{\Omega}_2$ (Methods). The coupling strength between |T, ↓↓⟩ and |T, ↓↑⟩ is $\sqrt{2}\Omega_1$, and the coupling strength between |T, ↓↑⟩ and |T, ↑↑⟩ is $\eta\sqrt{2}\Omega_1$. **d**, The measured pair oscillation frequency $\tilde{\Omega}_2$ varies with inverse scattering volume. Error bars are the fit uncertainty of the oscillation frequency. The solid and dashed lines are the predictions based on the AbI and PsP calculations, respectively (Methods). **e**, The wavefunction overlap η as a function of inverse scattering volume, inferred from the measured two-photon Rabi frequency of **d**. Error bars are the estimated statistical uncertainty of all experimental parameters combined with the fit uncertainty of $\tilde{\Omega}_2$. The solid and dashed lines are the overlap calculated using AbI and PsP wavefunctions, respectively (Methods).

sensitive to the wavefunction overlap η between the interacting and non-interacting states (Methods). The two-atom RF Rabi frequency also has a $\sqrt{2}$ enhancement above the single-atom coupling Ω_1 due to constructive interference among pure spin-triplet states. In Fig. 3d, we compare the observed pair Rabi frequency to theoretical predictions for a range of inverse scattering volumes, and find excellent agreement. This measurement allows us to extract η directly, as shown in Fig. 3e. The observed agreement between theory and experiment demonstrates coherent control of the system and success of both the AbI and regularized PsP to predict the interacting wavefunction.

A final experiment probes the lifetime τ of the *p*-wave interacting pairs. In the absence of three-body recombination, the lifetimes are limited for ^{40}K by inelastic two-body collisions of pairs of atoms at short interatomic separation (Fig. 4a), with a characteristic lifetime $\tau_d \approx 3.4$ ms (refs. [40,41]) (Methods). The pair lifetime is measured with a double-pulse sequence (inset of Fig. 4b) in which |T, ↑↑⟩ pairs are created, held for a variable hold time and transferred back to |T, ↓↓⟩. The survival lifetime is extracted from the exponential decay of the ensemble magnetization, as shown in Fig. 4b for two different magnetic fields. Even though the strong lattice confinement increases the on-site atomic density, we find lifetimes in excess of 50 ms, which is 50 times longer than previously observed for free-space dimers[34]. The relatively long lifetime of the 199.2 G condition can be understood by its reduced probability (χ) for having small internuclear separation $r \ll a_{ho}$ where relaxation processes are strongest (Fig. 4c,d). Both AbI and regularized PsP wavefunctions allow us to calculate χ; as shown in Fig. 4e, these show excellent agreement with measured lifetimes using the simple relation $\tau = \tau_d/\chi$, with a τ_d independent of lattice confinement. The observed agreement across all interaction energies demonstrates the full suppression of three-body recombination, the absence of band relaxation, the validity of both the AbI and PsP wavefunctions, and the calculation of τ_d. Figure 4f plots χ versus $a_{ho}^3/v(\mathcal{E})$, which emphasizes the applicability of the wavefunctions to any *p*-wave system, even those (such as ^{6}Li[20,21,23,38,42]) without the dipolar relaxation channel present in ^{40}K |T, ↑↑⟩ pairs[40].

The observation, control and comprehensive understanding of strong *p*-wave interactions demonstrated here illuminate a path towards the assembly of new many-body states of matter. In a full lattice model, the measured $U_p^{(i)}$ calibrates the on-site interaction, while lattice depth controls tunnelling between sites. For sufficiently small

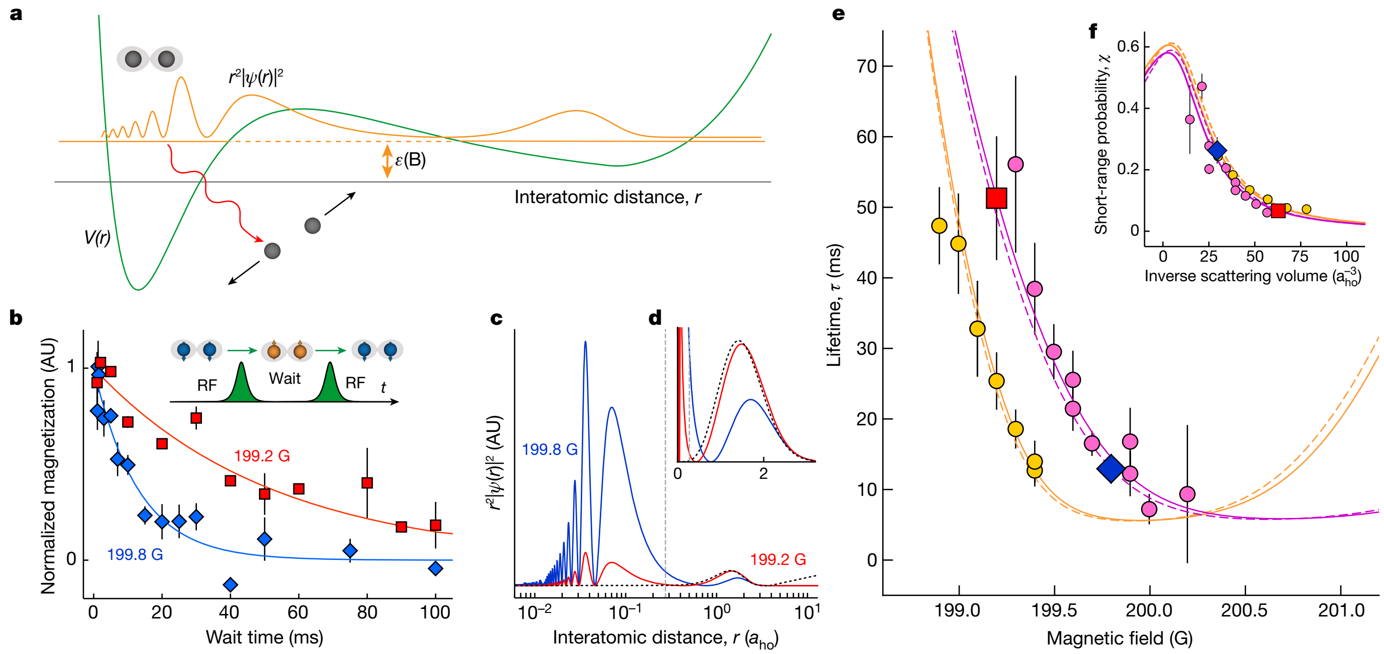

Fig. 4 | Lifetime of *p*-wave interacting pairs. **a**, The lifetime of an interacting ^{40}K *p*-wave pair is limited by dipolar relaxation of the metastable dimer at short range. The Born–Oppenheimer potential energy (green) has a short-range interaction component and a long-range component due to harmonic confinement (not to scale). **b**, The lifetime of BR$^{(1)}$ pairs is measured as the $1/e$ decay time of the normalized magnetization for the experimental sequence described in the text (inset). Data are shown for trap angular frequency $\omega = 2\pi \times 129(2)$ kHz at magnetic fields 199.20(1) G (red) and 199.80(1) G (blue) with lifetimes 51(9) ms and 13(2) ms, respectively. Error bars show the standard deviation of repeated measurements. **c**, The probability density $r^2|\psi|^2$ exhibits distinct short- and long-range components. Coloured solid lines correspond to AbI wavefunctions for experimental conditions in **b**; the vertical dashed line indicates the distance up to which the short-range probability χ is calculated (see Supplementary Information). **d**, Probability densities of **c** with linear scaling in interatomic distance. The black dotted wavefunctions give the non-interacting $n_{\rm rel} = 1$ oscillator state for comparison. **e**, The measured lifetime decreases for magnetic fields closer to the unitary limit. Shown are data for harmonic trap angular frequencies $\omega = 2\pi \times 90(2)$ kHz (yellow) and $\omega = 2\pi \times 129(2)$ kHz (pink). The square and diamond markers correspond to the temporal data shown in **b**. Error bars are the fit uncertainty of the $1/e$ decay time. The lines are theory predictions based on the AbI wavefunctions (solid) and PsP wavefunctions (dashed). **f**, The variation of the measured short-range probability χ with inverse scattering volume. Error bars are calculated from the uncertainty in τ. Solid and dashed lines are predictions from AbI and PsP calculations, respectively, where χ attains a maximum value near the unitary point (Methods).

tunnelling strength, losses might continue to be suppressed either through the quantum Zeno effect[27] or by the energetic gaps to triple on-site occupation[28]. In two dimensions, the $U_p^{(0)} < 0$ interactions observed here in BR$^{(0)}$ in the orbital angular momentum projection $|M_L| = 1$ channel are the precursors of a topological superfluid[4–8] that features gapless chiral edge modes or 'Majorana zero modes' in vortex cores[11,29]. These modes are non-Abelian anyons that are predicted to offer unique opportunities for topological quantum computation and robust quantum memories[2,11,29]. Even a metastable many-body state would allow for the study of topological states in a quenched *p*-wave superfluid[43]. The $U_p^{(1)} > 0$ interactions observed here are the precursors of orbital magnetism known from transition metal oxides[44], as well as orbitally ordered Mott insulators in a multiband Fermi–Hubbard model[8,45,46]. Strong orbital interactions demonstrated in this work can also be used to engineer low-entropy states in a multiband lattice system[47] and a full gate-based control of entangled many-body states[48]. Finally, the universal nature of the observed interaction energies indicates that they would be reproduced in other ultracold *p*-wave systems such as ^{6}Li[20,21,38,42] and ultracold fermionic molecules[49,50].

Online content

Any methods, additional references, Nature Portfolio reporting summaries, source data, extended data, supplementary information, acknowledgements, peer review information, details of author contributions and competing interests, and statements of data and code availability are available at https://doi.org/10.1038/s41586-022-05405-6.

1. Volovik, G. *The Universe in a Helium Droplet, International Series of Monographs on Physics* (Clarendon Press, 2003).
2. Ivanov, D. A. Non-Abelian statistics of half-quantum vortices in *p*-wave superconductors. *Phys. Rev. Lett.* **86**, 268–271 (2001).
3. Mizushima, T. et al. Symmetry-protected topological superfluids and superconductors: from the basics to ^{3}He. *J. Phys. Soc. Jpn* **85**, 022001 (2016).
4. Botelho, S. S. & Sá de Melo, C. A. R. Quantum phase transition in the BCS-to-BEC evolution of *p*-wave Fermi gases. *J. Low Temp. Phys.* **140**, 409–428 (2005).
5. Gurarie, V., Radzihovsky, L. & Andreev, A. V. Quantum phase transitions across a *p*-wave Feshbach resonance. *Phys. Rev. Lett.* **94**, 230403 (2005).
6. Cheng, C.-H. & Yip, S.-K. Anisotropic Fermi superfluid via *p*-wave Feshbach resonance. *Phys. Rev. Lett.* **95**, 070404 (2005).
7. Levinsen, J., Cooper, N. R. & Gurarie, V. Strongly resonant *p*-wave superfluids. *Phys. Rev. Lett.* **99**, 210402 (2007).
8. Zhao, E. & Liu, W. V. Orbital order in Mott insulators of spinless *p*-band fermions. *Phys. Rev. Lett.* **100**, 160403 (2008).
9. Tewari, S., Das Sarma, S., Nayak, C., Zhang, C. & Zoller, P. Quantum computation using vortices and majorana zero modes of a p_x+ip_y superfluid of fermionic cold atoms. *Phys. Rev. Lett.* **98**, 010506 (2007).
10. Zhang, C., Tewari, S. & Das Sarma, S. Bell's inequality and universal quantum gates in a cold-atom chiral fermionic *p*-wave superfluid. *Phys. Rev. Lett.* **99**, 220502 (2007).
11. Nayak, C., Simon, S. H., Stern, A., Freedman, M. & Das Sarma, S. Non-Abelian anyons and topological quantum computation. *Rev. Mod. Phys.* **80**, 1083–1159 (2008).
12. Jona-Lasinio, M., Pricoupenko, L. & Castin, Y. Three fully polarized fermions close to a *p*-wave Feshbach resonance. *Phys. Rev. A* **77**, 043611 (2008).
13. D'Incao, J. P., Esry, B. D. & Greene, C. H. Ultracold atom-molecule collisions with fermionic atoms. *Phys. Rev. A* **77**, 052709 (2008).
14. Nishida, Y., Moroz, S. & Son, D. T. Super Efimov effect of resonantly interacting fermions in two dimensions. *Phys. Rev. Lett.* **110**, 235301 (2013).
15. Wang, Y., D'Incao, J. P. & Greene, C. H. Universal three-body physics for fermionic dipoles. *Phys. Rev. Lett.* **107**, 233201 (2011).
16. Martin, M. J. et al. A quantum many-body spin system in an optical lattice clock. *Science* **341**, 632–636 (2013).
17. Lemke, N. D. et al. *p*-wave cold collisions in an optical lattice clock. *Phys. Rev. Lett.* **107**, 103902 (2011).

18. Regal, C. A., Ticknor, C., Bohn, J. L. & Jin, D. S. Tuning *p*-wave interactions in an ultracold Fermi gas of atoms. *Phys. Rev. Lett.* **90**, 053201 (2003).
19. Suno, H., Esry, B. D. & Greene, C. H. Recombination of three ultracold fermionic atoms. *Phys. Rev. Lett.* **90**, 053202 (2003).
20. Zhang, J. et al. *p*-wave Feshbach resonances of ultracold ^{6}Li. *Phys. Rev. A* **70**, 030702 (2004).
21. Schunck, C. H. et al. Feshbach resonances in fermionic ^{6}Li. *Phys. Rev. A* **71**, 045601 (2005).
22. Günter, K., Stöferle, T., Moritz, H., Köhl, M. & Esslinger, T. *P*-wave interactions in low-dimensional fermionic gases. *Phys. Rev. Lett.* **95**, 230401 (2005).
23. Chevy, F. et al. Resonant scattering properties close to a *p*-wave Feshbach resonance. *Phys. Rev. A* **71**, 062710 (2005).
24. Waseem, M., Yoshida, J., Saito, T. & Mukaiyama, T. Unitarity-limited behavior of three-body collisions in a *p*-wave interacting Fermi gas. *Phys. Rev. A* **98**, 020702 (2018).
25. Li, X. & Liu, W. V. Physics of higher orbital bands in optical lattices: a review. *Rep. Prog. Phys.* **79**, 116401 (2016).
26. Dutta, O. et al. Non-standard Hubbard models in optical lattices: a review. *Rep. Prog. Phys.* **78**, 066001 (2015).
27. Han, Y.-J. et al. Stabilization of the *p*-wave superfluid state in an optical lattice. *Phys. Rev. Lett.* **103**, 070404 (2009).
28. Fedorov, A. K., Yudson, V. I. & Shlyapnikov, G. V. *p*-wave superfluidity of atomic lattice fermions. *Phys. Rev. A* **95**, 043615 (2017).
29. Alicea, J. New directions in the pursuit of Majorana fermions in solid state systems. *Rep. Prog. Phys.* **75**, 076501 (2012).
30. Chang, Y.-T., Senaratne, R., Cavazos-Cavazos, D. & Hulet, R. G. Collisional loss of one-dimensional fermions near a *p*-wave Feshbach resonance. *Phys. Rev. Lett.* **125**, 263402 (2020).
31. Marcum, A. S., Fonta, F. R., Mawardi Ismail, A. & O'Hara, K. M. Suppression of three-body loss near a *p*-wave resonance due to quasi-1D confinement. Preprint at https://doi.org/10.48550/arXiv.2007.15783 (2020).
32. Idziaszek, Z. Analytical solutions for two atoms in a harmonic trap: *p*-wave interactions. *Phys. Rev. A* **79**, 062701 (2009).
33. Kanjilal, K. & Blume, D. Nondivergent pseudopotential treatment of spin-polarized fermions under one- and three-dimensional harmonic confinement. *Phys. Rev. A* **70**, 042709 (2004).
34. Gaebler, J. P., Stewart, J. T., Bohn, J. L. & Jin, D. S. *P*-wave Feshbach molecules. *Phys. Rev. Lett.* **98**, 200403 (2007).
35. Stöferle, T., Moritz, H., Günter, K., Köhl, M. & Esslinger, T. Molecules of fermionic atoms in an optical lattice. *Phys. Rev. Lett.* **96**, 030401 (2006).
36. Hartke, T., Oreg, B., Jia, N. & Zwierlein, M. Quantum register of fermion pairs. *Nature* **601**, 537–541 (2022).
37. Müller, T., Fölling, S., Widera, A. & Bloch, I. State preparation and dynamics of ultracold atoms in higher lattice orbitals. *Phys. Rev. Lett.* **99**, 200405 (2007).
38. Fuchs, J. et al. Binding energies of ^{6}Li *p*-wave Feshbach molecules. *Phys. Rev. A* **77**, 053616 (2008).
39. Busch, T., Englert, B.-G., Rzażewski, K. & Wilkens, M. Two cold atoms in a harmonic trap. *Found. Phys.* **28**, 549–559 (1998).
40. Ticknor, C., Regal, C. A., Jin, D. S. & Bohn, J. L. Multiplet structure of Feshbach resonances in nonzero partial waves. *Phys. Rev. A* **69**, 042712 (2004).
41. Ahmed-Braun, D. J. M. et al. Probing open- and closed-channel *p*-wave resonances. *Phys. Rev. Res.* **3**, 033269 (2021).
42. Inada, Y. et al. Collisional properties of *p*-wave Feshbach molecules. *Phys. Rev. Lett.* **101**, 100401 (2008).
43. Foster, M. S., Gurarie, V., Dzero, M. & Yuzbashyan, E. A. Quench-induced floquet topological *p*-wave superfluids. *Phys. Rev. Lett.* **113**, 076403 (2014).
44. Tokura, Y. & Nagaosa, N. Orbital physics in transition-metal oxides. *Science* **288**, 462–468 (2000).
45. Imada, M., Fujimori, A. & Tokura, Y. Metal-insulator transitions. *Rev. Mod. Phys.* **70**, 1039–1263 (1998).
46. Mamaev, M. et al. Collective *p*-wave orbital dynamics of ultracold fermions. *Phys. Rev. Lett.* **127**, 143401 (2021).
47. Bakr, W. S. et al. Orbital excitation blockade and algorithmic cooling in quantum gases. *Nature* **480**, 500–503 (2011).
48. Mamaev, M., Thywissen, J. H. & Rey, A. M. Quantum computation toolbox for decoherence-free qubits using multi-band alkali atoms. *Adv. Quantum Technol.* **3**, 1900132 (2020).
49. Marco, L. D. et al. A degenerate Fermi gas of polar molecules. *Science* **363**, 853–856 (2019).
50. Duda, M. et al. Long-lived fermionic Feshbach molecules with tunable *p*-wave interactions. Preprint at https://doi.org/10.48550/arXiv.2202.06940 (2022).

Methods

Spin and motional wavefunctions

The single-atom spin states ↑ and ↓ used in the experiment are adiabatically connected to the low-field $m_f = -9/2$ and $m_f = -7/2$ states of the ground hyperfine manifold of ^{40}K with total spin $f = 9/2$. The pair spin wavefunctions are given by $|\mathrm{S}, \uparrow\downarrow\rangle = (|\downarrow, \uparrow\rangle - |\uparrow, \downarrow\rangle)/\sqrt{2}$, $|\mathrm{T}, \uparrow\uparrow\rangle = |\uparrow, \uparrow\rangle$, $|\mathrm{T}, \downarrow\downarrow\rangle = |\downarrow, \downarrow\rangle$ and $|\mathrm{T}, \uparrow\downarrow\rangle = (|\downarrow, \uparrow\rangle + |\uparrow, \downarrow\rangle)/\sqrt{2}$. The motional states of the pair are defined in terms of spherical harmonic oscillator eigenstates for the relative atomic separation r (see Supplementary Information),

$$\begin{aligned} |E\rangle &= |\mathcal{N}, L, M_L\rangle, \\ E &= \hbar\omega\left(2\mathcal{N} + L + \frac{3}{2}\right). \end{aligned} \tag{1}$$

Here $\mathcal{N} \in \{0, 1, 2, \ldots\}$ is the radial excitation number, $L \in \{0, 1, 2, \ldots\}$ is the relative angular momentum and $M_L \in \{-L, \ldots, L\}$ is the angular momentum projection along the magnetic field axis. The total number of motional excitations can also be characterized by a single quantum number $n_{\mathrm{rel}} = 2\mathcal{N} + L = 1, 3, \ldots$, as $L = 1$ for p-wave interactions.

State preparation and read-out

The degenerate Fermi gas is a balanced spin mixture of ^{40}K in its lowest two hyperfine spin states created via sympathetic optical evaporation with ^{87}Rb in a crossed optical dipole trap[51,52]. After evaporation, the gas typically contains 2×10^5 atoms with temperature $0.1\,T_{\mathrm{F}}$, where T_{F} is the Fermi temperature.

The optical lattice potential is formed by orthogonal retro-reflected laser beams of wavelengths $\lambda_{xy} = 1{,}054$ nm in the x–y plane and $\lambda_z = 1{,}064$ nm along the z-axis with beam waists $(w_x, w_y, w_z) = (60, 60, 85)$ µm. The potential depth of the lattice is parameterized in terms of the recoil energy of the xy lattice beams, $E_{\mathrm{R}} = \hbar^2 k_L^2/2m$, where $k_L = 2\pi/\lambda_{xy}$ and m is the mass of a ^{40}K atom. The harmonic trap angular frequency of a lattice site ω is given by $\hbar\omega = E_{\mathrm{R}}\sqrt{4V_{\mathrm{L}}/E_{\mathrm{R}}}$, where V_{L} is the lattice depth. The lattice depths are regulated to be isotropic and are verified by comparing amplitude-modulation spectroscopy to band structure. We estimate the lattice anisotropy to be less than 2%.

Isolated pairs of atoms in the $|\mathrm{S}, \uparrow\downarrow\rangle\ |0\rangle_{\mathrm{rel}}$ state are created by ramping the lattice depth to $10\,E_{\mathrm{R}}$ in 150 ms, waiting for 50 ms and then suppressing tunnelling with a fast ramp to $60\,E_{\mathrm{R}}$ in 250 µs. In situ fluorescence imaging with a quantum gas microscope verifies that approximately 10% of the sites are doubly occupied. The lattice depth is then ramped to $200\,E_{\mathrm{R}}$ in 100 ms, and the magnetic field along the z lattice direction is ramped to 197 G in 150 ms. Atom pairs in the $|\mathrm{S}, \uparrow\downarrow\rangle\ |0\rangle_{\mathrm{rel}}$ state are transferred to the $|\mathrm{T}, \downarrow\downarrow\rangle\ |1\rangle_{\mathrm{rel}}$ state by a 65 µs Raman π-pulse which is detuned from the Zeeman splitting by a motional quanta and the on-site s-wave interaction energy of the $|\mathrm{S}, \uparrow\downarrow\rangle\ |0\rangle_{\mathrm{rel}}$ state.

To perform state read-out, the magnetic field is first ramped (in 50 ms) to 195 G where the atom pairs are weakly interacting. The resultant absolute spin populations of the ↑ and ↓ states are measured via absorption imaging after band mapping and a 15 ms time of flight. A double shutter imaging technique enables measurement of both spin populations in a single experimental realization.

Raman excitation

The Raman coupling is generated by two linearly polarized beams in the x–y plane whose propagation directions are oriented at 30° and 60°, respectively, with the x and y lattice directions. A small angular deviation from the x–y plane allows excitations along the z motional degree of freedom, and thus $M_L = 0$ features are present in the spectra. The single-photon detuning of each Raman laser beam is stabilized to −50.1 GHz from the D2 transition and is chosen to avoid undesired photo-association of pairs of ^{40}K atoms at a single site.

RF spectroscopy

After preparing the non-interacting $|\mathrm{T}, \downarrow\downarrow\rangle\ |1\rangle_{\mathrm{rel}}$ pair state, the lattice depth and magnetic field are ramped sequentially in 50 ms to their operating values as indicated in the main text. The RF spectroscopy implements the hyperbolic secant pulse shape, which is defined by the following time-dependent detuning $\delta(t)$ about the central frequency f_{RF}, and Rabi frequency $\Omega(t)$:

$$\Omega(t) = \Omega_0\,\mathrm{sech}\,(2\beta t/T_{\mathrm{p}}) \tag{2}$$

$$\delta(t) = \delta_{\mathrm{c}} + \delta_{\mathrm{m}}\tanh\,(2\beta t/T_{\mathrm{p}}). \tag{3}$$

Here, Ω_0 is the peak Rabi frequency at resonance, which is essentially the single-particle Rabi frequency Ω_1. Note that in the Rabi oscillation measurements, the Rabi frequency is fixed as a constant of $\Omega(t) = \Omega_1$. In the expression of the detuning above, δ_{m} is the maximum absolute detuning with respect to the central detuning of $\delta_{\mathrm{c}}/(2\pi) = f_{\mathrm{RF}} - f_{\mathrm{ZS}}$, and T_{p} is the characteristic pulse time. The dimensionless tuning parameter β sets the relative sharpness of the sweep. Typical experimental parameters are $\delta_{\mathrm{m}} = 2\pi \times 2.5$ kHz, $\Omega_0 = 2\pi \times 8.8$ kHz, $\beta = 0.05$ and $T_{\mathrm{p}} = 2$ ms.

Feshbach resonance

In free space, $|\mathrm{T}, \uparrow\uparrow\rangle$ pairs of atoms have a p-wave magnetic Feshbach resonance at 198.30 G for $M_L = \pm 1$, and 198.80 G for $M_L = 0$. In the effective range approximation, the energy-dependent scattering volume $\upsilon(\mathcal{E})$ for each collisional channel is given by

$$\upsilon(\mathcal{E}) \approx \left[\frac{1}{\upsilon_{\mathrm{bg}}\left(1 - \frac{\Delta}{B - B_0}\right)} + \frac{\mu\mathcal{E}}{\hbar^2 R(B)}\right]^{-1}, \tag{4}$$

where υ_{bg} is the background scattering volume, Δ is the resonance width, B_0 is the resonant magnetic field in free space, B is the applied magnetic field, $\mu = m/2$ is the reduced mass and $R(B)$ is the field-dependent effective range given by the linear expression $R(B) = R_0[1 + (B - B_0)/\Delta_r]$. The resonance parameters for $M_L = 0$ are $\upsilon_{\mathrm{bg}} = -(108.0a_0)^3$, $\Delta = -19.89$ G, $R_0 = 49.4\,a_0$ and $\Delta_r = 21.1$ G. The resonance parameters for $M_L = \pm 1$ are $\upsilon_{\mathrm{bg}} = -(107.35a_0)^3$, $\Delta = -19.54$ G, $R_0 = 48.9a_0$ and $\Delta_r = 21.7$ G[41].

Pseudopotential

The p-wave interaction between two identical atoms can be computed via a regularized PsP[32,33,53] given by

$$V_p(\mathbf{r}) = \frac{12\pi\hbar^2\upsilon(\mathcal{E})}{m}\overleftarrow{\nabla}_{\mathbf{r}}\delta^{(3)}(\mathbf{r})\overrightarrow{\nabla}_{\mathbf{r}}\frac{1}{2}\frac{\partial^2}{\partial r^2}r^2, \tag{5}$$

where $\mathbf{r}$ is the relative position of the atoms and $r = |\mathbf{r}|$ their separation, $\delta^{(3)}$ is the three-dimensional Dirac delta function and $\overleftarrow{\nabla}_{\mathbf{r}}$, $\overrightarrow{\nabla}_{\mathbf{r}}$ are left-/right-acting gradients, respectively. In principle, the energy-dependent scattering volume $\upsilon(\mathcal{E})$ is different for the $M_L = \pm 1$ and $M_L = 0$ channels due to dipolar interactions. Thus, the PsP should be separated into terms with spatial derivatives acting in the x–y plane and z direction (as the magnetic field points along z) with different scattering volumes. However, this does not lead to coupling between the M_L channels. Therefore, the energies of the different channels are simply given by the solution of the isotropic case with the appropriate scattering volume.

An isotropic scattering volume permits an analytic solution for the energy $\mathcal{E}$, which is given implicitly by[32,33]

$$-\frac{a_{\mathrm{ho}}^3}{\upsilon(\mathcal{E})} = 8\frac{\Gamma\left(\frac{5}{4} - \frac{\mathcal{E}}{2\hbar\omega}\right)}{\Gamma\left(-\frac{1}{4} - \frac{\mathcal{E}}{2\hbar\omega}\right)} \tag{6}$$

where $\Gamma(z)$ is the gamma function. The corresponding spatial wavefunction can be written as[33]

$$\psi_{\rm int}(r)=\begin{cases}\mathcal{A}\dfrac{r}{a_{\rm ho}}e^{-\frac{r^2}{2a_{\rm ho}^2}}U\left(-\dfrac{\mathcal{E}}{2\hbar\omega}+\dfrac{5}{4},\dfrac{5}{2},\dfrac{r^2}{a_{\rm ho}^2}\right) & r>r_{\rm cut}\\ 0 & r\le r_{\rm cut}\end{cases}\tag{7}$$

where $\mathcal{A}$ is a normalization constant, $U(a, b, z)$ is the confluent hypergeometric function of the second kind and $r_{\rm cut} = 50\ a_0$ is a cut-off used to treat the divergence as $r \to 0$, obtained by comparing directly to AbI wavefunction calculations (see Supplementary Information).

Anharmonic corrections

The anharmonic correction to the PsP energy is approximated using first-order perturbation theory. We compute the expectation value of fourth-order Taylor expansion terms of the lattice trapping potential about the centre of a lattice site (see Supplementary Information). The resulting correction is

$$\Delta\mathcal{E}_{\rm anharmonic}=-E_R\left(\frac{1}{10a_{\rm ho}^4}\int_0^\infty {\rm d}r\,r^6|\psi_{\rm int}(r)|^2+\frac{1}{2a_{\rm ho}^2}\int_0^\infty {\rm d}r\,r^4|\psi_{\rm int}(r)|^2-\frac{17}{8}\right).\tag{8}$$

The perturbative treatment may break down if the relative motional branches are split by exactly an integer multiple of $\hbar\omega$, which allows a resonant anharmonicity-enabled coupling to the centre-of-mass motion. This resonant coupling then strongly mixes the motional degrees of freedom resulting in a further splitting of each branch[54]. We do not observe such structure experimentally, although we do not rule out its presence. However, the good agreement and scaling collapse for our data suggest that such effects are relatively small for the parameter ranges probed.

Pair Rabi oscillations

The Rabi oscillation spin dynamics of an interacting pair is captured by the following three-level model (see Supplementary Information),

$$\hat{H}^{\rm pair}=\frac{\hbar}{2}\begin{pmatrix}0 & \sqrt{2}\Omega_1 & 0\\ \sqrt{2}\Omega_1 & -U_p^{(1)}/\hbar & \sqrt{2}\Omega_1\eta\\ 0 & \sqrt{2}\Omega_1\eta & 0\end{pmatrix},\tag{9}$$

written in the basis of $\{|T,\downarrow\downarrow\rangle|1\rangle_{\rm rel}, |T,\uparrow\downarrow\rangle|1\rangle_{\rm rel}, |T,\uparrow\uparrow\rangle|\psi_{\rm int}\rangle_{\rm rel}\}$. Here Ω_1 is the single-photon Rabi frequency of the RF drive, while η is a spatial wavefunction overlap between the non-interacting and interacting states (see Supplementary Information),

$$\eta={}_{\rm rel}\langle\psi_{\rm int}|1\rangle_{\rm rel}=\int_0^\infty {\rm d}r\,r^2\psi_{\rm int}^*(r)\psi_{\rm rel}^{(n_{\rm rel}=1)}(r),$$

where

$$\psi_{\rm rel}^{(n_{\rm rel}=1)}(r)=\left(\frac{8}{3\pi^{1/2}a_{\rm ho}^3}\right)^{1/2}\frac{r}{a_{\rm ho}}\exp\left(-\frac{r^2}{2a_{\rm ho}^2}\right).\tag{10}$$

In the limit of $U_p^{(1)} \gg \hbar\Omega_1$, dynamics under this Hamiltonian are characterized by a single frequency:

$$\widetilde{\Omega}_2=\frac{\sqrt{(U_p^{(1)}/\hbar)^2+8(1+\eta^2)\Omega_1^2}-U_p^{(1)}/\hbar}{4}.\tag{11}$$

Experimental measurements extract η from the above equation, as all other parameters are independently measured.

Lifetime prediction

The lifetime τ of the interacting state is limited by inelastic decay due to dissociation of the pair into unbound atoms. Dipolar interactions couple the interacting state $|{\rm T},\uparrow\uparrow\rangle|1\rangle_{\rm rel}|0\rangle_{\rm CM}$ to a lossy dimer state at short interatomic separation, which undergoes dissociation with a characteristic lifetime $\tau_{\rm d}$. The dimer lifetime for $M_L = +1$ and $M_L = -1$ is $\tau_{+1} = 8.7$ ms and $\tau_{-1} = 2.1$ ms, respectively[41]. Our motional excitation is predominantly along a single Cartesian lattice direction in the $\hat{\mathbf{x}}\,\hat{\mathbf{y}}$ plane, which corresponds to an equal superposition of $M_L = +1, -1$; the characteristic lifetime is thus $\tau_{\rm d}^{-1} = (\tau_{+1}^{-1} + \tau_{-1}^{-1})/2$, such that $\tau_{\rm d} = 3.4$ ms. The actual lifetime further depends on the short-range wavefunction probability χ. We theoretically predict χ from the interacting wavefunctions by computing the overall probability up to a characteristic threshold (see Supplementary Information). At all probed magnetic fields, we see a clear distinction between short- and long-range components, such as in Fig. 4c. The threshold is chosen to capture the short-range portion of the wavefunction only.

Data availability

Source data are provided with this paper.

51. Edge, G. J. A. et al. Imaging and addressing of individual fermionic atoms in an optical lattice. *Phys. Rev. A* **92**, 063406 (2015).
52. Anderson, R. et al. Conductivity spectrum of ultracold atoms in an optical lattice. *Phys. Rev. Lett.* **122**, 153602 (2019).
53. Omont, A. On the theory of collisions of atoms in Rydberg states with neutral particles. *J. Phys. France* **38**, 1343–1359 (1977).
54. Mentink, J. & Kokkelmans, S. Two interacting atoms in an optical lattice site with anharmonic terms. *Phys. Rev. A* **79**, 032709 (2009).

Acknowledgements We acknowledge insightful discussions with F. Chevy and S. Zhang and helpful manuscript comments from J. Bohn, A. Kaufman and R. Learn. This work is supported by the AFOSR grants FA9550-19-1-0275, FA9550-19-1-7044 and FA9550-19-1-0365, by ARO W911NF-15-1-0603, by the NSF's JILA-PFC PHY-1734006 and PHY-2012125 grants, by NIST and by NSERC.

Author contributions V.V., P.X., F.C., C.J.F. and J.H.T. developed the experimental techniques and collected the data. V.V., P.X., M.M., F.C. and C.J.F. performed the data analysis. M.M., T.B., C.J.F., J.P.D'I. and A.M.R. developed the theoretical models. All authors contributed to writing the manuscript.

Competing interests The authors declare no competing interests.

Additional information

Supplementary information The online version contains supplementary material available at https://doi.org/10.1038/s41586-022-05405-6.

Correspondence and requests for materials should be addressed to Cora J. Fujiwara, Ana Maria Rey or Joseph H. Thywissen.

Peer review information *Nature* thanks Xiaopeng Li and the other, anonymous, reviewer(s) for their contribution to the peer review of this work.